OPEN ACCESS

ISSN: 2835-9496

Ruppen IC, et al. (2025): 718
Ameri J Clin Med Re, 2025; 5(1): 100175
DOI: 10.71010/AJCMR.2025-e175

Research Article

American Journal of Clinical and Medical Research

# Whole-Body Magnetic Resonance Imaging in the Evaluation of Bone Metastases and Multiple Myeloma: A Pictorial Essay

**Ian Caldeira Ruppen [1*], Leandro Hideki Otani[2], Jamile Diogo de Araujo[2], Felicia Satie Ibuki Otani[2], Vitor Augusto Olivari do Carmo[1], Lara Beatriz Dallaqua Bitiati[1], Gabriel Petermann[3], Alana Reigota da Costa Rosa[1], Geórgia Verona Cruz[2], Geovani Almeida Gois[4], Larissa da Rosa Piccoli[1], Marcela Castrequini Guimarães do Vale[1], Rafaela Castrequini Guimarães do Vale[1], Juliano Rodrigues Narvaes[1], Haloany Maola Chitolina[1], Rafaela Beatriz Siqueira[1], Paschoal Carlos Figueiredo Morelli[1], Pedro Henrique Rodrigues Flamengo[1], Alice Naomi Macedo[1], Fernanda Aburjaili Mendes[1], Ana Renatha Porto Melo Bandeira[6], Amanda Luisa Pires Barichello[1]**

[1]Centro Universitário Ingá – Uningá, Maringá, PR, Brazil
[2]Instituto Maringá de Imagem, Maringá, PR, Brazil
[3]Faculdade Cesumar – Unicesumar, Maringá, PR Brazil
[4]Universidade Federal do Maranhão, Brazil
[5]Universidad Autónoma San Sebastián - UASS, Paraguay

***Corresponding author:** Ian Caldeira Ruppen, Centro Universitário Ingá - Uningá, Maringá, Paraná, Brazil. **Email:** Ian2ruppen@gmail.com; **ORCID:** https://orcid.org/0000-0003-1706-1662

**Citation:** Ruppen IC, Otani LH, de Araujo JD, Ibuki Otani FS, Olivari do Carmo VA, et al. (2025) Whole-Body Magnetic Resonance Imaging in the Evaluation of Bone Metastases and Multiple Myeloma: A Pictorial Essay. Clin Med Re: AJCMR-175.

**Received Date:** 1 Januarry, 2025; **Accepted Date:** 07 January, 2025; **Published Date:** 10 January, 2025

## Introduction

In recent years, several articles have studied the application of whole-body magnetic resonance imaging (MRI) for oncological staging, yielding promising results for different types of primary lesions (1-7). Technological advancements in MRI equipment have allowed the development of new techniques, notably diffusion-weighted imaging, which has generated significant scientific interest in the research and monitoring of metastases. The objective of our study is to demonstrate the application of this examination in screening for secondary bone lesions and staging multiple myeloma.

## Methods

We evaluated 18 cases of whole-body MRI conducted at our institution during 2012. The most illustrative cases were selected, considering their clinical history, correlation with various imaging modalities, and the clinical applicability of the method.

## Exam Protocol

The exam was performed on a 1.5 Tesla device (Optima 450w, GE). Coronal T1- and STIR-weighted images were obtained in three blocks (head and thorax, abdomen, pelvis, and thighs). Axial diffusion-weighted images with a B-value of 600 to 750 were also acquired. For these blocks, either the body or torso coil was used. Subsequently, the patient was positioned in the spine coil, and sagittal T1- and fat-saturated T2-weighted images were acquired in two blocks (cervicothoracic and thoracolumbar spine). The coronal image blocks were fused into a single image encompassing the entire body from the cephalic region to the distal third of the thighs.

## Clinical Case 1

A 47-year-old female patient (ILTR) was recently diagnosed with breast cancer. A bone scan for staging showed uptake at L3. The scintigraphic report suggested correlation with radiological studies to differentiate between secondary processes and degenerative changes. A whole-body MRI was requested to evaluate the uptake area at L3 (Figs. 1 and 2), which revealed bone lesions in the vertebral bodies of T3, L3, the right ilium, and the greater trochanter, all showing restricted diffusion and consistent with secondary involvement.

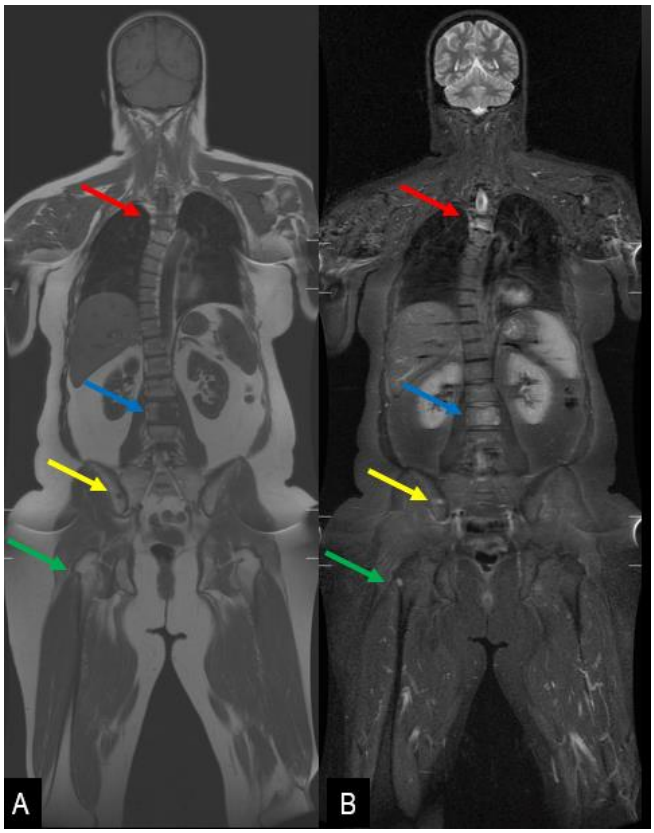


**Figure 1:** Coronal T1-weighted (A) and STIR (B) images demonstrate a nodular lesion in the vertebral body of L3 (blue arrow), corresponding to the scintigraphic finding. Additional lesions were identified in the vertebral body of T3 (red arrow), the right ilium (yellow arrow), and the right greater trochanter (green arrow), all suspected of secondary involvement.

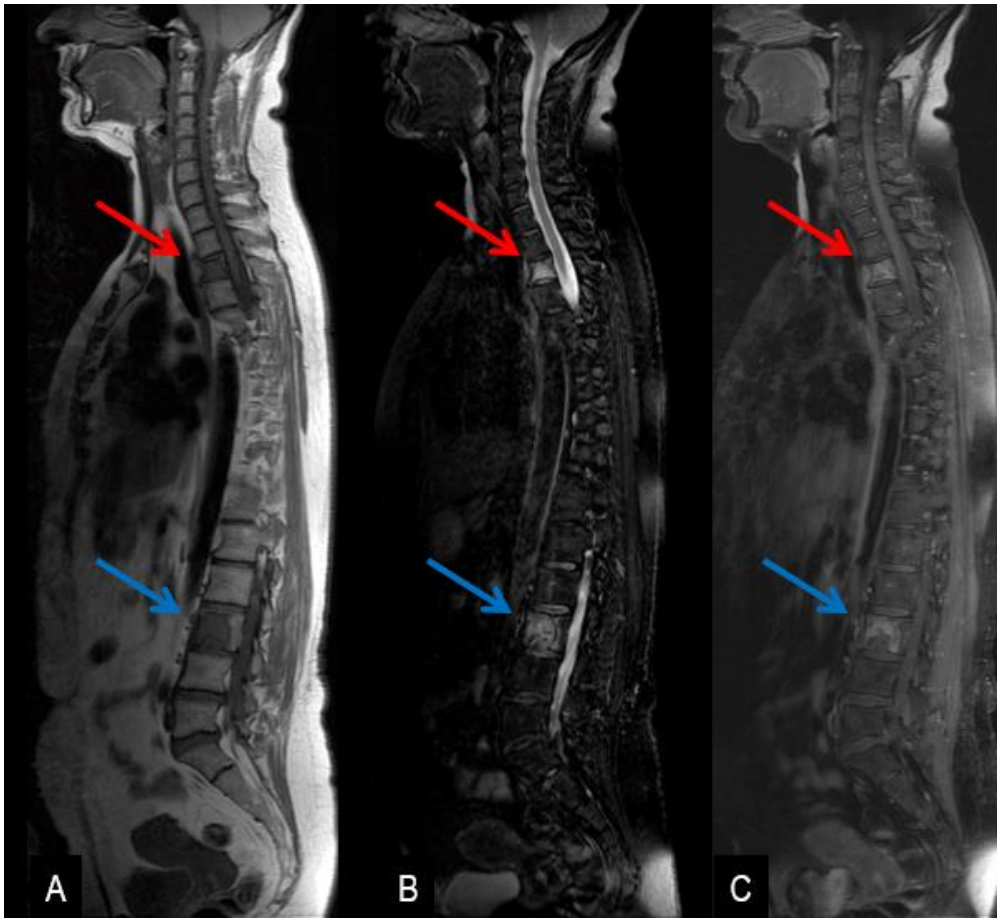


**Figure 2:** Sagittal T1-weighted (A), STIR (B), and post-contrast T1-weighted (C) images show nodular lesions in the vertebral bodies of T3 (red arrow) and L3 (blue arrow), consistent with secondary lesions.

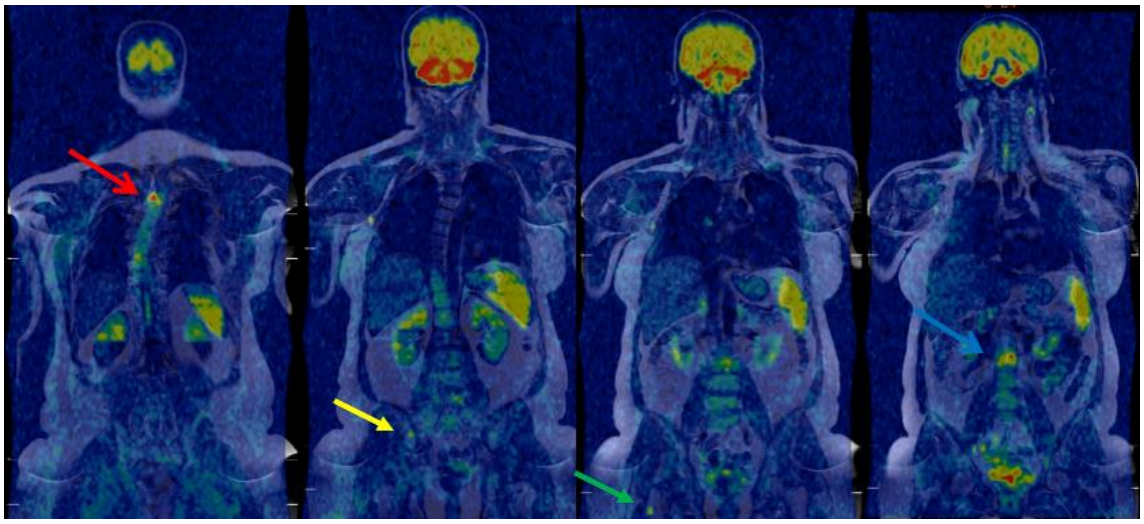

**Figure 3:** Fusion of diffusion-weighted images with coronal T1-weighted images. The areas of restricted diffusion are displayed on a color scale. Lesions in the vertebral bodies of T3 (red arrow), L3 (blue arrow), the right ilium (yellow arrow), and the right greater trochanter (green arrow) exhibit restricted diffusion, suggesting high cellularity and supporting the hypothesis of secondary lesions. In this case, the whole-body MRI characterized the L3 scintigraphic alteration as a secondary lesion, ruling out degenerative or traumatic lesions as the cause of the uptake. The exam also identified additional secondary lesions, providing a comprehensive assessment of bone involvement.

## Clinical Case 2

A male patient (JCRL) with a history of prostate cancer and a known diagnosis of bone metastases underwent whole-body MRI, which showed multiple diffuse nodular lesions throughout the spine and pelvis (Figs. 4 and 5), consistent with secondary lesions. Additionally, an area of sclerosis in the anterior and right lateral mandibular regions was identified on axial T1-weighted images (Fig. 6). The patient had a history of mandibular osteonecrosis, likely related to bisphosphonate use (8).

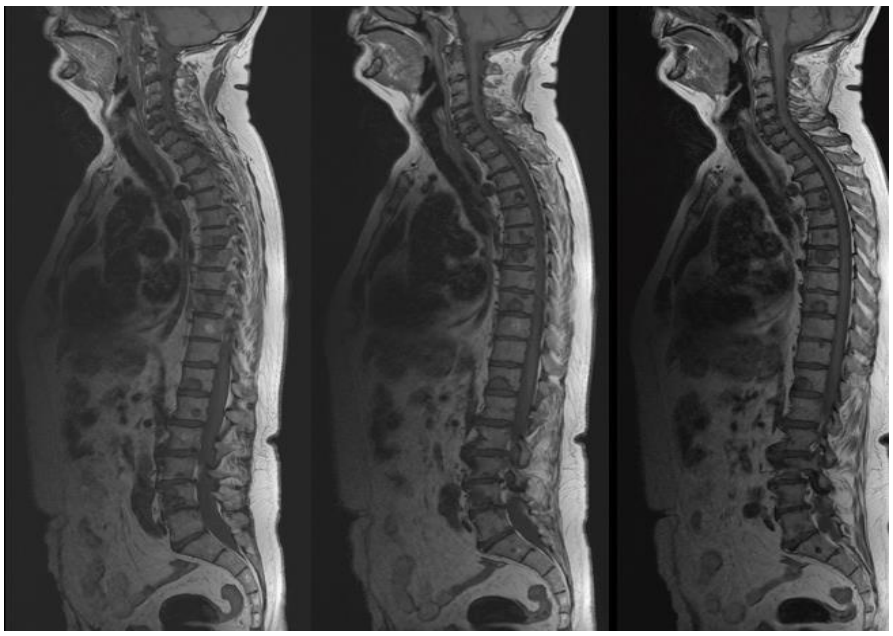

**Figure 4:** Sagittal T1-weighted images demonstrate diffuse nodular lesions throughout the spine, consistent with secondary lesions.

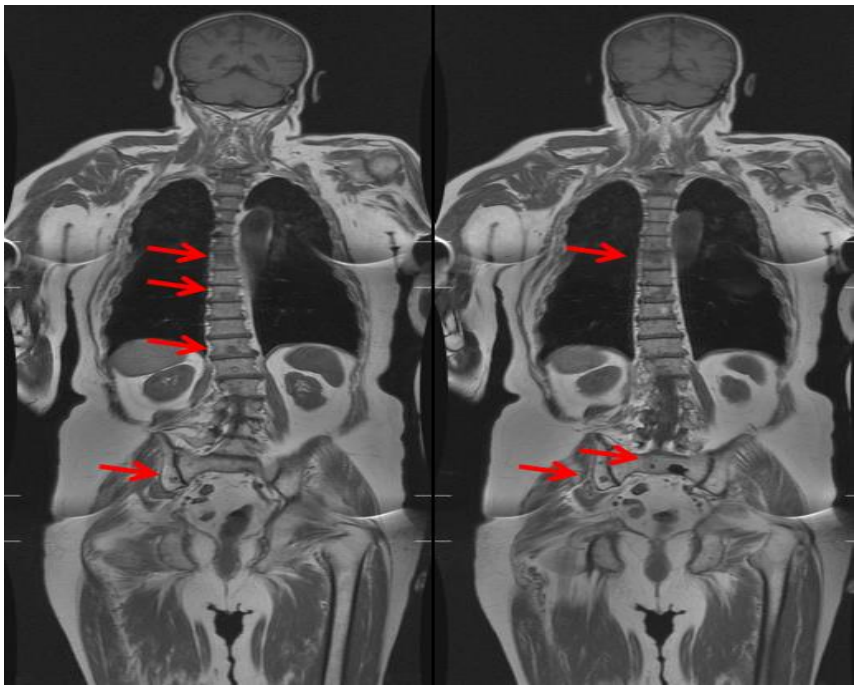

**Figure 5:** Coronal T1-weighted images demonstrate lesions in the spine and pelvis (red arrows), consistent with secondary lesions.

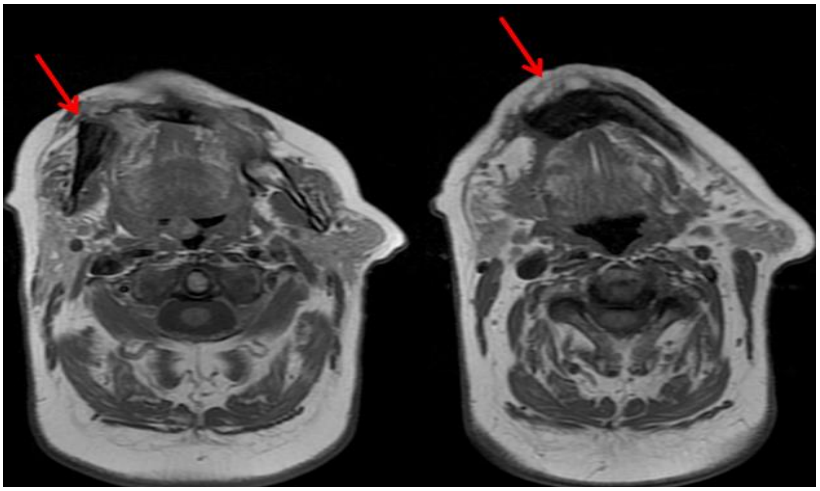

**Figure 6:** Axial T1-weighted images demonstrate areas of sclerosis in the anterior and right lateral regions of the mandible, consistent with the patient's history of osteonecrosis.

In this case, whole-body MRI demonstrated disseminated secondary lesions across bony structures. Although already diagnosed, one of the treatment-related complications (mandibular osteonecrosis) was also characterized in the study, highlighting its potential for identifying bone complications and guiding targeted investigations.

## Clinical Case 3

HC, 49 years old, male, with clinical-laboratory suspicion of multiple myeloma. Initial radiographic evaluations of the skull, spine, pelvis, and long bones (Fig. 7) did not demonstrate lesions suspicious for bone involvement. Therefore, a whole-body MRI was indicated for further investigation. The study revealed extensive diffuse bone infiltration, characterized by areas of reduced T1 signal and high STIR signal, evident in the spine (Fig. 8), pelvis, and long bones (Fig. 9).

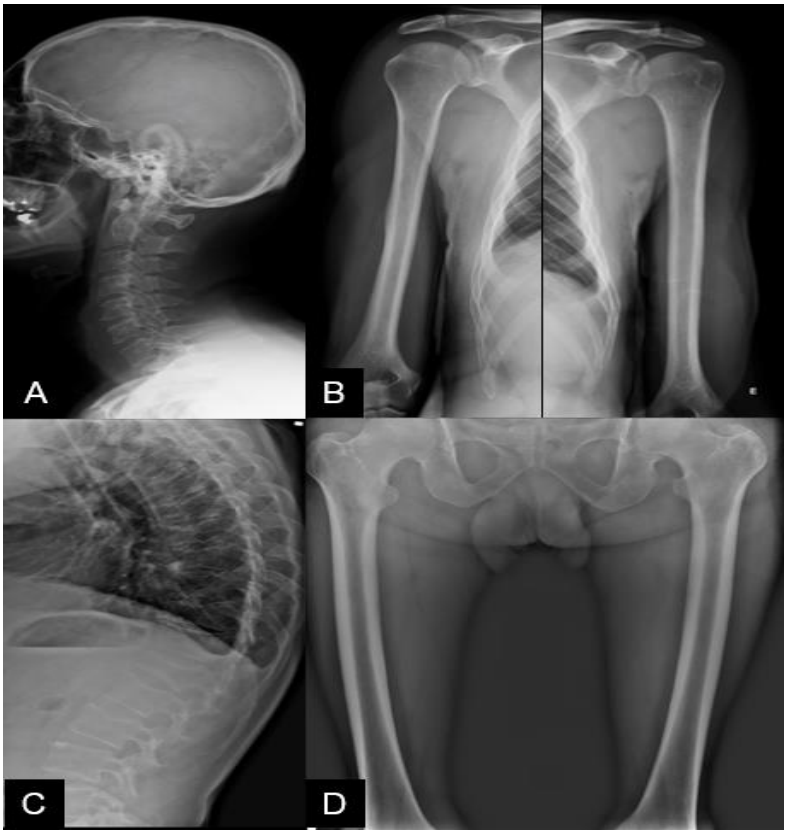


**Figure 7:** Radiographs of the skull and cervical spine (A), humeri (B), thoracic spine (C), and femurs (D) do not demonstrate osteolytic lesions. Thoracic spine images (C) show reduced height in several vertebral bodies in this segment.

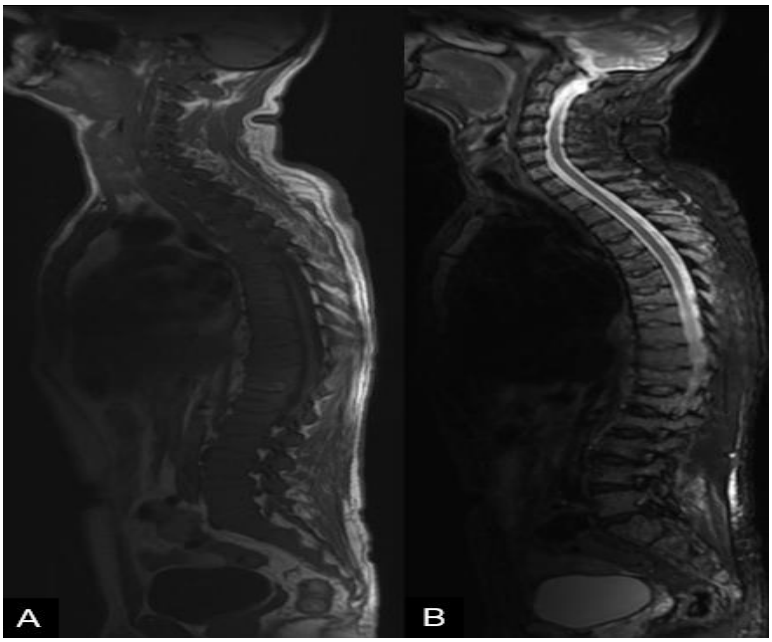


**Figure 8:** Sagittal whole-spine T1-weighted (A) and STIR (B) images show extensive marrow signal alterations in vertebral bodies, characterized by hypointensity in T1 and hyperintensity in STIR. Reduced height of several vertebral bodies in the thoracic and lumbar regions was also observed.

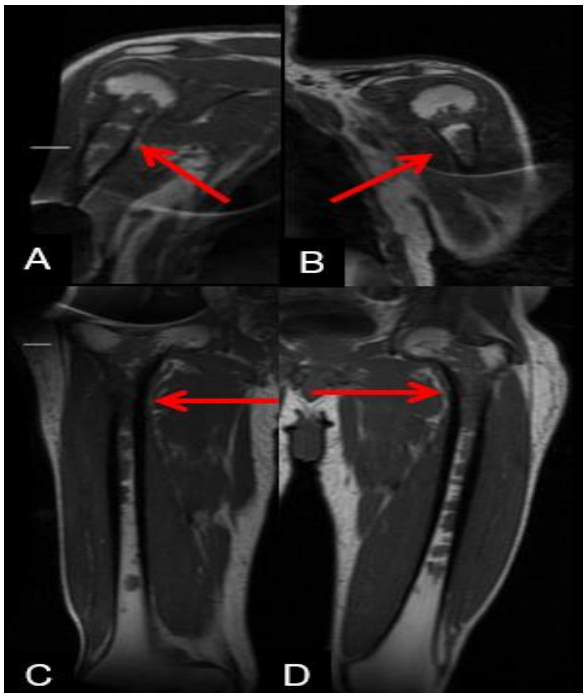


**Figure 9:** Coronal T1-weighted images encompassing the proximal thirds of the right (A) and left (B) humeri and the right (C) and left (D) femoral shafts show areas of marrow infiltration, characterized by hypointense foci.

Whole-body MRI was crucial in this case, as the initial radiographic evaluation was normal. This situation is common, as radiographs detect myeloma-related lesions only when 50% of the bone mineral content is lost. Various studies also demonstrate the superiority of MRI over radiographs in evaluating this pathology (10).

### Clinical Case 4

JM, 78 years old, male, with a history of an insufflative lesion in the L1 vertebral body, recently operated and diagnosed histologically with multiple myeloma/plasmacytoma. Following this finding, further investigation with whole-body MRI was conducted to identify other bone lesions.

The study revealed other infiltrative lesions located in the T4 and L5 vertebral bodies (Fig. 10).

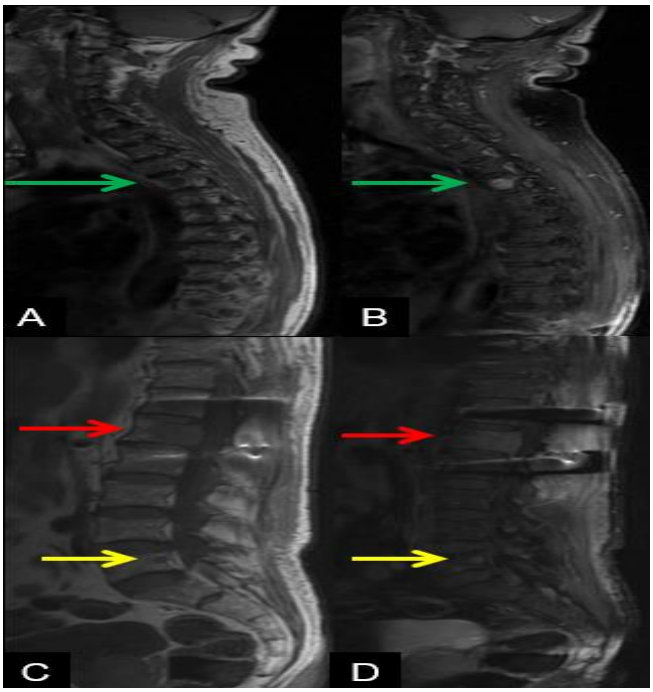


**Figure 10:** Sagittal images of the cervicothoracic spine in T1-weighted (A) and post-contrast (B) sequences, and thoracolumbar spine in T1-weighted (C) and post-contrast (D) sequences. In addition to the lesion in L1 (red arrow), other lesions were identified in T4 (green arrow) and L5 (yellow arrow).

The multiplicity of lesions confirmed the diagnosis of multiple myeloma over solitary plasmacytoma.

### Clinical Case 5

JB, female, diagnosed with multiple myeloma, presenting with low back pain. Whole-body MRI was requested to evaluate areas of bone infiltration and better investigate the back pain.

The MRI showed nodular lesions in the T11, L2, L3, and L5 vertebral bodies (Fig. 11), consistent with disease involvement. It also demonstrated acute fractures in vertebral bodies from T10 to L2, some with slight posterior wall retropulsion, but without contact with the spinal cord cone (Fig. 12).

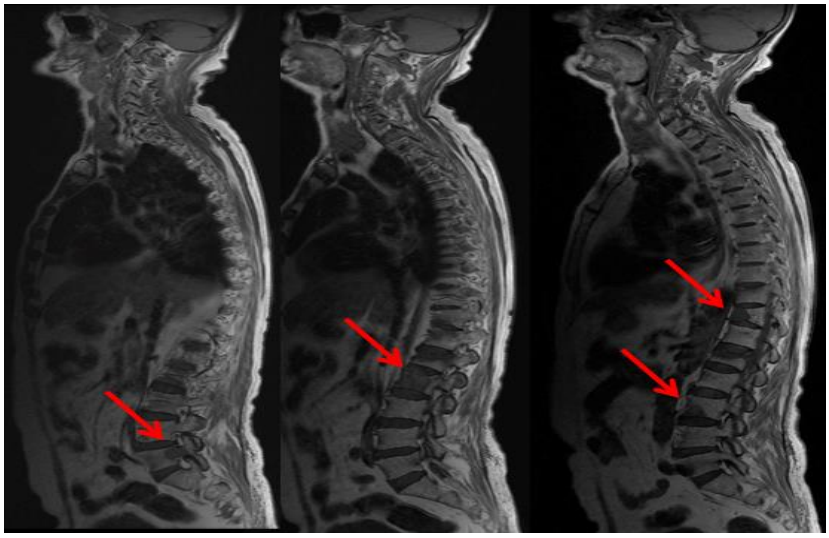

**Figure 11:** Sagittal whole-spine T1-weighted images show multiple nodular lesions in the T11, L2, L3, and L5 vertebral bodies, consistent with multiple myeloma involvement.

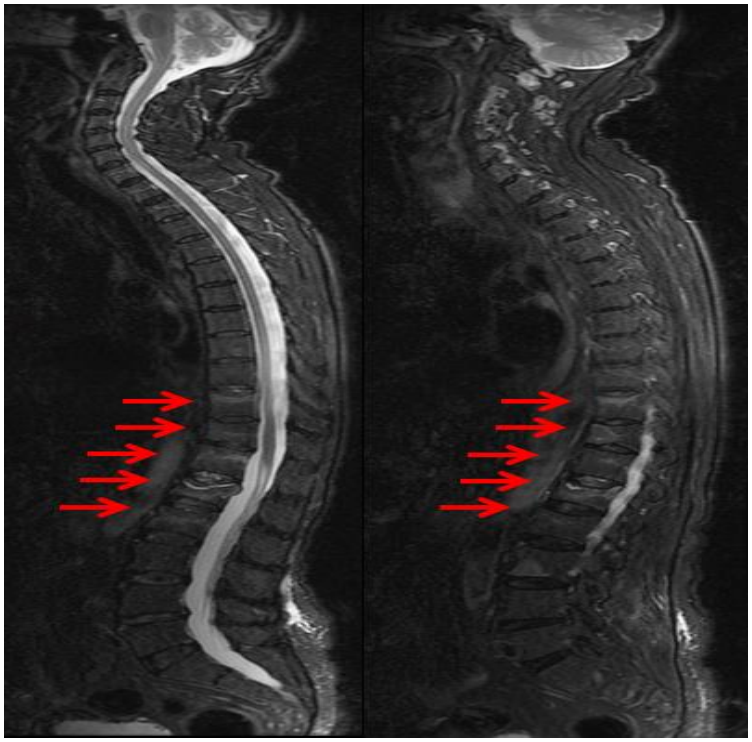

**Figure 12:** Sagittal whole-spine STIR images show compressive fractures of the superior endplates of vertebral bodies from T10 to L2. A slight posterior-superior wall angulated retropulsion in L1 is noted, but without contact with the spinal cord cone.

Whole-body MRI not only demonstrated areas of multiple myeloma involvement but also revealed acute compressive vertebral fractures, a significant complication of this pathology. It also allowed for the evaluation of the spinal canal and the relationship between the fractures and the spinal cord and cone.

## Clinical Case 6

VAM, 75 years old, male. Patient with a history of testicular pain for one month. He sought another service where an ultrasound revealed a solid nodule in the left testicle (Fig. 13). The patient underwent surgery, with orchiectomy, and the histopathological analysis revealed a testicular plasmacytoma. Based on this diagnosis, whole-body MRI was requested to investigate bone involvement.

The MRI revealed diffuse bone lesions involving the spine (Fig. 14), costal arches, humeri, and femurs (Fig. 15). Some spinal lesions had insufflative characteristics, and the lesion involving the right costal arches exhibited an extraosseous soft tissue component. Given the diffuse bone involvement illustrated by whole-body MRI, the possibility of multiple myeloma presenting as a testicular plasmacytoma was considered.

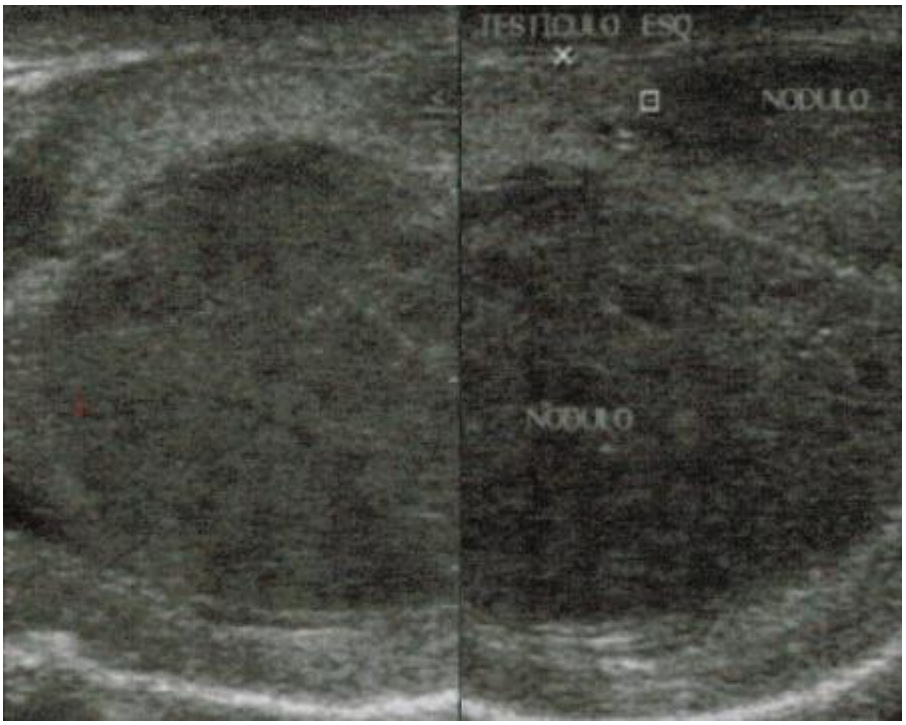


**Figure 13:** Ultrasound shows a solid, hypoechoic nodule in the left testicle.

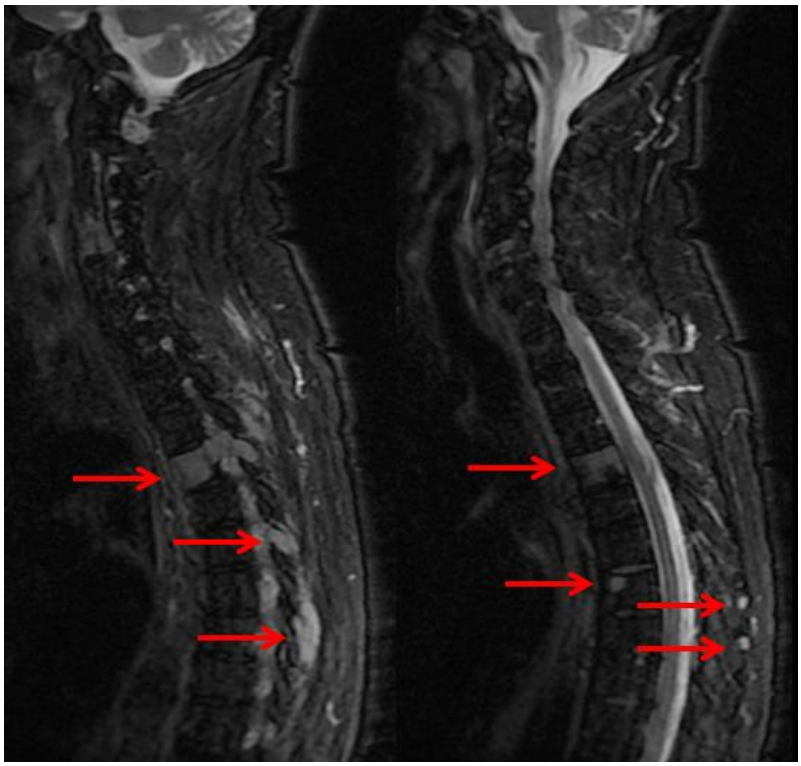

**Figure 14:** Sagittal STIR spine images show multiple diffuse bone lesions throughout the spine, some with insufflative characteristics.

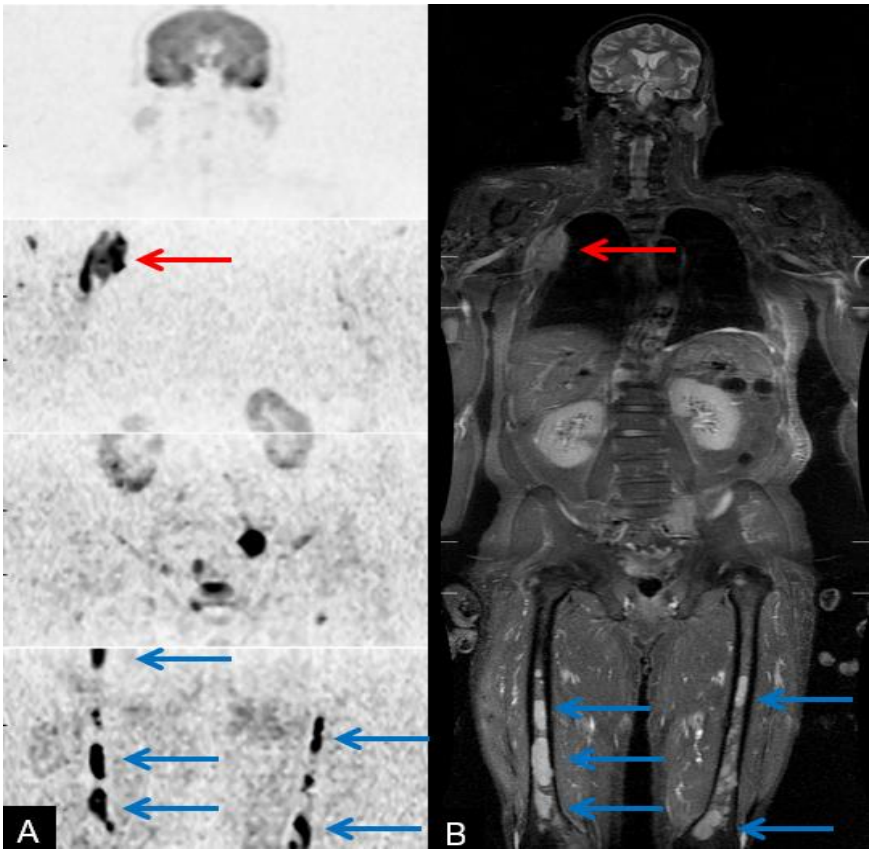


**Figure 15:** Coronal diffusion sequence reformatted image (A) and coronal STIR images (B) show bone lesions with an extraosseous soft tissue component in the right costal arches (red arrow) and multiple lesions in the femoral shafts (blue arrows). The lesions exhibited high cellularity, represented by altered areas illustrated in the diffusion sequence.

## Conclusion

Several studies have demonstrated the advantages of using whole-body MRI for evaluating bone metastases and multiple myeloma (1-7, 11), particularly in cases where reduced radiation exposure is desired (e.g., children and pregnant women) and for patients contraindicated for contrast (11).

However, these same studies emphasize the need for further research, particularly comparing MRI with other available methods and considering the variability of bone marrow in different scenarios (e.g., age groups, post-chemotherapy and radiotherapy treatments, and use of hematopoietic-stimulating medications) (11).

## References

1. CASCINI, G.; FALCONE, C.; GRECO, C.; BERTUCCI, B.; CIPULLO, S.; TAMBURRINI, O. Whole-body magnetic resonance imaging for detecting bone metastases: comparison with bone scintigraphy. Radiol Med, v. 113, n. 8, p. 1157-1170, 2008.
2. SOHAIB, S. A.; COOK, G.; ALLEN, S. D.; HUGHES, M.; EISEN, T.; GORE, M. Comparison of whole-body MRI and bone scintigraphy in the detection of bone metastases in renal cancer. Br J Radiol, v. 82, p. 632-639, 2009.
3. OHLMANN-KNAFO, S.; KIRSCHBAUM, M.; FENZL, G.; PICKUTH, D. Diagnostic value of whole-body MRI and bone scintigraphy in the detection of osseous metastases in patients with breast cancer - A Prospective Double-Blinded Study at two Hospital Centers. Rofo, v. 181, p. 255-263, 2009.
4. TAKENAKA, D.; OHNO, Y.; MATSUMOTO, K.; AOYAMA, N.; ONISHI, Y.; KOYAMA, H.; NOGAMI, M.; YOSHIKAWA, T.; MATSUMOTO, S.; SUGIMURA, K. Detection of bone metastases in non-small cell lung cancer patients: comparison of whole-body diffusion-weighted imaging (DWI), whole-body MR imaging without and with DWI, whole-body FDG-PET/CT, and bone scintigraphy. J Magn Reson Imaging, v. 30, p. 298-308, 2009.
5. BALLIU, E.; BOADA, M.; PELÁEZ, I.; VILANOVA, J. C.; BARCELÓ-VIDAL, C.; RUBIO, A.; GALOFRÉ, P.; CASTRO, A.; PEDRAZA, S. Comparative study of whole-body MRI and bone scintigraphy for the detection of bone metastases. Clin Radiol, v. 65, p. 989-996, 2010.
6. GU, J.; CHAN, T.; ZHANG, J.; LEUNG, A. Y. H.; KWONG, Y. L.; KHONG, P. L. Whole-Body Diffusion-Weighted Imaging: The Added Value to Whole-Body MRI at Initial Diagnosis of Lymphoma. AJR, v. 197, p. W384-W391, 2011.
7. LEUCOVET, F. E.; EL MOUEDDEN, J.; COLLETTE, L.; COCHE, E.; DANSE, E.; JAMAR, F.; MACHIELS, J. P.; VANDE BERG, B.; OMOUMI, P.; TOMBAL, B. Can whole-body magnetic resonance imaging with diffusion-weighted imaging replace Tc 99m bone scanning and computed tomography for single-step detection of metastases in patients with high-risk prostate cancer Eur Urol, v. 62, p. 68-75, 2012.
8. JANOVSKA, Z. Bisphosponate-related osteonecrosis of the jaws. A severe side effect of bisphosphonate therapy. Acta Medica, v. 55, p. 111-115, 2012.
9. ÁLVAREZ-MÚGICA, M.; MONZÓN, A. J.; VÁZQUEZ, V. B.; ANDREA, C. A.; GÓMEZ, J. M. F.; ÁLVAREZ, R. C. G.; SEJAS, F. J. R. Secondary Testicular Plasmocytoma. Arch Esp Urol, v. 60, p. 99-102, 2007.
10. SCHMIDT, G. P.; REISER, M. F.; BAUR-MELNYK, A. Whole-body imaging of the musculoskeletal system: the value of MR imaging. Skeletal Radiol, v. 36, p. 1109-1119, 2007.
11. PADHANI, A. R.; KOH, D. M.; COLLINS, D. J. Whole-Body Diffusion-weighted MR Imaging in Cancer: Current Status and Research Directions. Radiology, v. 263, p. 700-718, 2011.